

1 **A conceptual model-based sediment connectivity assessment for patchy agricultural catchments**

2 Pedro V. G. Batista<sup>1\*</sup>, Peter Fiener<sup>2</sup>, Simon Scheper<sup>1,3</sup>, Christine Alewell<sup>1</sup>

3 <sup>1</sup>Department of Environmental Sciences, Universität Basel, Bernoullistrasse 30, 4056, Basel,  
4 Switzerland.

5 <sup>2</sup>Institute for Geography, Universität Augsburg, Alter Postweg 118, 86159, Augsburg, Germany.

6 <sup>3</sup>Dr. Simon Scheper – Research | Consulting | Teaching, Eickhorst 3, 29413 Dähre, Germany

7

8 \*Corresponding author. Now at Institute for Geography, Universität Augsburg, Alter Postweg 118,  
9 86159, Augsburg, Germany, pedro.batista@geo.uni-augsburg.de

10

11 **Abstract**

12 The accelerated sediment supply from agricultural soils to riverine and lacustrine environments leads to  
13 negative off-site consequences. In particular, the sediment connectivity from agricultural land to surface  
14 waters is strongly affected by landscape patchiness and the linear structures that separate field parcels  
15 (e.g. roads, tracks, hedges, and grass buffer strips). Understanding the interactions between these  
16 structures and sediment transfer is therefore crucial for minimising off-site erosion impacts. Although  
17 soil erosion models can be used to understand lateral sediment transport patterns, model-based  
18 connectivity assessments are hindered by the uncertainty in model structures and input data. In specific,  
19 the representation of linear landscape features in numerical soil redistribution models is often  
20 compromised by the spatial resolution of the input data and the quality of the process descriptions. Here  
21 we adapted the WaTEM/SEDEM model using high resolution spatial data (2 m x 2 m) to analyse the  
22 sediment connectivity in a very patchy mesoscale catchment (73 km<sup>2</sup>) of the Swiss Plateau. We used a  
23 global sensitivity analysis to explore model structural assumptions about how linear landscape features  
24 (dis)connect the sediment cascade, which allowed us to investigate the uncertainty in the model  
25 structure. Furthermore, we compared model simulations of hillslope sediment yields from five sub-  
26 catchments to tributary sediment loads, which were calculated with long-term water discharge and  
27 suspended sediment measurements. The sensitivity analysis revealed that the assumptions about how  
28 the road network (dis)connects the sediment transfer from field blocks to water courses had a much  
29 higher impact on modelled sediment yields than the uncertainty in model parameters. Moreover, model  
30 simulations showed a higher agreement with tributary sediment loads when the road network was  
31 assumed to directly connect sediments from hillslopes to water courses. Our results ultimately illustrate  
32 how a high-density road network combined with an effective drainage system increases sediment  
33 connectivity from hillslopes to surface waters in agricultural landscapes. This further highlights the  
34 importance of considering linear landscape features and model structural uncertainty in soil erosion and  
35 sediment connectivity research.

36

## 37 **1 Introduction**

38 Rainfall events on sloped surfaces continuously displace soil particles, which are transported downslope  
39 as sediments. These sediments are then stored and remobilised several times before conceivably  
40 reaching surface waters. Accordingly, the sediment cascade is a natural and potentially long  
41 geomorphological process (Fryirs, 2013). However, the accelerated sediment supply from agricultural  
42 soils to riverine and lacustrine environments leads to negative off-site consequences. Specifically,  
43 phosphorus-rich and pollutant-bound particulate matter from arable land is associated to the  
44 eutrophication and contamination of water courses (Krasa et al., 2019; Lacey et al., 2021). Extreme  
45 erosion events in agricultural fields are also linked to the occurrence of muddy floods (Boardman, 2020)  
46 and to damages to downstream infrastructure (Bauer et al., 2019). Therefore, understanding how and  
47 when sediment is transferred from agricultural fields to different landscape compartments is imperative  
48 to reduce off-site erosion impacts.

49 The degree with which a system facilitates sediment transfer within its internal compartments is defined  
50 by Heckmann et al. (2018) as sediment connectivity. This concept can be further distinguished into a  
51 structural component, associated to the semi-static spatial configuration of the landscape; and a  
52 functional one, which emerges as a dynamic property of the hydro-sedimentological system  
53 (Wainwright et al., 2011). Connectivity theory therefore provides a framework to rethink the sediment  
54 delivery problem (Fryirs, 2013; Parsons et al., 2009) and to understand the complex spatiotemporal  
55 processes that regulate sediment transport.

56 In agricultural landscapes, sediment connectivity is strongly affected by the patchiness of the land use  
57 configuration, and the presence of linear features between field parcels (e.g. hedges, grass buffer strips,  
58 and roads) (Alder et al., 2015; Bakker et al., 2008; Chartin et al., 2013; Fiener et al., 2011; Remund et  
59 al., 2021; Van Oost et al., 2000). The importance of landscape patchiness in regulating sediment transfer  
60 is specifically relevant in areas where a large number of small fields, separated by linear structures,  
61 create a complex hydrological system. However, the experimental analysis of sediment connectivity at  
62 catchment scale is challenging, as it involves measuring both internal soil redistribution processes and  
63 cascading sediment transport rates. The interaction between landscape patchiness, linear structures, and  
64 sediment connectivity is therefore not addressed by the typical setup of experimental erosion studies,  
65 which either focus on small erosion plots or catchment sediment yields (Fiener et al., 2019).

66 Due to the difficulties in measuring the processes that affect sediment movement at catchment and  
67 landscape scale, it is common practice to analyse connectivity with modelling approaches (Nunes et al.,  
68 2018). These usually rely on high-resolution process-based models, assuming they are able to represent  
69 connectivity dynamics (Baartman et al., 2020); semi-qualitative indices (Borselli et al., 2008; Cavalli et  
70 al., 2013); or more recently, the coupling of conceptual models with probability theory (Mahoney et al.,  
71 2020a, 2020b). In specific, the use of process-based soil erosion and sediment transport models might  
72 be an important pathway to improve our understanding of sediment connectivity (Nunes et al., 2018).

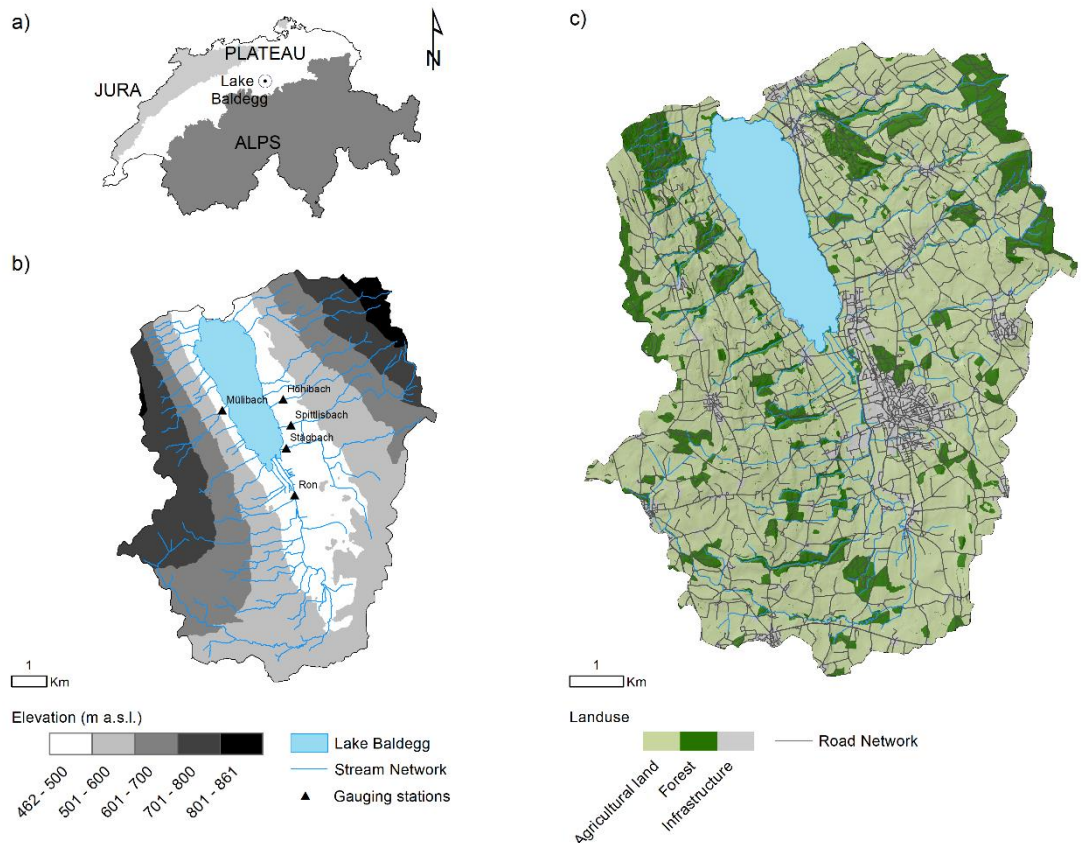
73 However, erosion models in general, and process-based models in particular, face two fundamental  
74 problems for representing sediment connectivity : (i) the input data requirements are large and uncertain,  
75 and model application is often restricted to small catchments with a maximum size of a few square  
76 kilometres (e.g. Baartman et al., 2020; Starkloff and Stolte, 2014; Wilken et al., 2017) and (ii) the  
77 implemented process descriptions, especially along linear landscape features and field boundaries, are  
78 weakly defined due to the aforementioned unavailability of experimental data. Borrelli et al. (2018)  
79 demonstrated how parcel-specific high resolution land cover and management data can improve soil  
80 erosion/sediment delivery models in patchy agricultural catchments.

81 Here, we aimed to (i) adapt a conceptual soil erosion and sediment delivery model with high spatial  
82 resolution data (2 m x 2 m) within a Monte Carlo framework; (ii) to analyse the sediment connectivity  
83 in a very patchy mesoscale catchment (73 km<sup>2</sup>) in Switzerland; and (iii) to perform a sensitivity analysis  
84 of model parameters and structural assumptions regarding how linear features (dis)connect the sediment  
85 cascade. Hence, we demonstrate how models can be used to understand the interaction between linear  
86 features, landscape patchiness, and sediment connectivity. This will contribute to increase our  
87 comprehension of relevant connectivity processes and our ability to develop appropriate measures for  
88 reducing off-site erosion impacts.

## 89 **2 Materials and methods**

### 90 **2.1 Study catchment**

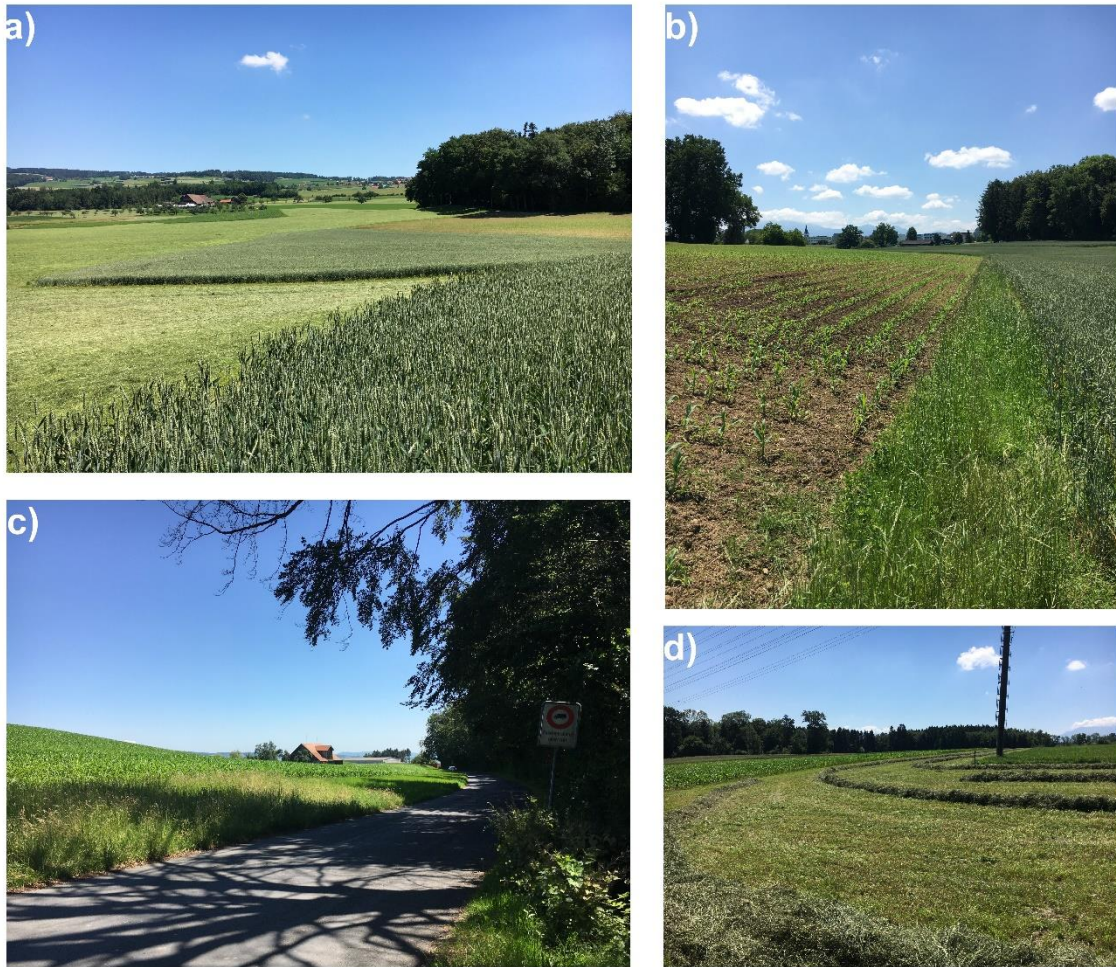
91 The study catchment consists of the contributing area of the Lake Baldegg, in the central Swiss Plateau  
92 (Figure 1). The lake has been extensively studied due to its hypertrophic waters, which have been  
93 artificially oxygenated since 1983 (e.g. Lavrieux et al., 2019; Müller et al., 2014; Teranes and  
94 Bernasconi, 2005). The eutrophication of the lake has been mostly linked to excessive phosphorus loads  
95 during the 20<sup>th</sup> century (Wehrli et al., 1997). Although water quality in the lake is currently improving  
96 (BAFU, 2016), the supply of phosphorus-rich sediment is still a concern to local authorities (von Arb et  
97 al., 2021; Stoll et al., 2019). The major advantage of the Baldegg catchment for this study is that a  
98 comprehensive hydrological data set is available based on an ongoing, long-term monitoring by the  
99 Department of Environment and Energy of the Canton of Lucerne.



100

101 Figure 1. a) Location of the Baldegg catchment; b) elevation, stream network, and location of  
 102 hydrological gauging stations; c) land use. Data source: Swisstopo (2018, 2020). Sub-catchment areas:  
 103 Höhibach (2.3 km<sup>2</sup>), Mülibach (1.6 km<sup>2</sup>), Stägibach (9.3 km<sup>2</sup>), Spittlisbach (3.8 km<sup>2</sup>), Ron (27.7 km<sup>2</sup>).

104 The Baldegg catchment has a total area of 73.2 km<sup>2</sup>, of which 5.2 km<sup>2</sup> are covered by the lake. The  
 105 remaining area is occupied by agricultural land (74%), forests (16%), and infrastructure (e.g.  
 106 settlements, developed areas, and roads) (10%) (Swisstopo, 2020) (Figure 1c). The agriculture consists  
 107 of intensively managed pastures and/or meadows, cereal production under crop rotation, permanent  
 108 grasslands, fruit orchards, and small vineyards (Lavrieux et al., 2019; Stoll et al., 2019). The majority  
 109 of the meadows are composed of a mixture of grasses and clover, which are harvested for silage, hay,  
 110 or barn feeding up to six times per year (von Arb et al., 2021). Agricultural field blocks, here delimited  
 111 by external boundaries (e.g. roads, water courses, and forests) (Bircher et al., 2019), have a median size  
 112 of 4.4 ha. However, smaller patches separated by hedges, tree lines, and grass buffer strips, are generally  
 113 found within the blocks (Figure 2).



114

115 Figure 2. Typical agricultural landscapes from the Baldegg catchment: a) Small arable and grassland  
 116 patches within larger field blocks, b) grass buffer strip between maize and wheat fields, c) wide grass  
 117 buffer strip between maize field and a vicinal road, d) freshly cut hay from a pasture between maize  
 118 fields.

119 The road network density in the Baldegg catchment is  $6.0 \text{ km km}^{-2}$ , which is approximately three times  
 120 higher than the stream density ( $1.9 \text{ km km}^{-2}$ ). Streams in the upper catchment are often incised, with  
 121 visible, yet not prominent, signs of bank erosion. A total of 22 channels flow into the Lake Baldegg, of  
 122 which five streams are monitored for water and sediment discharge by cantonal authorities, as described  
 123 in section 2.2.

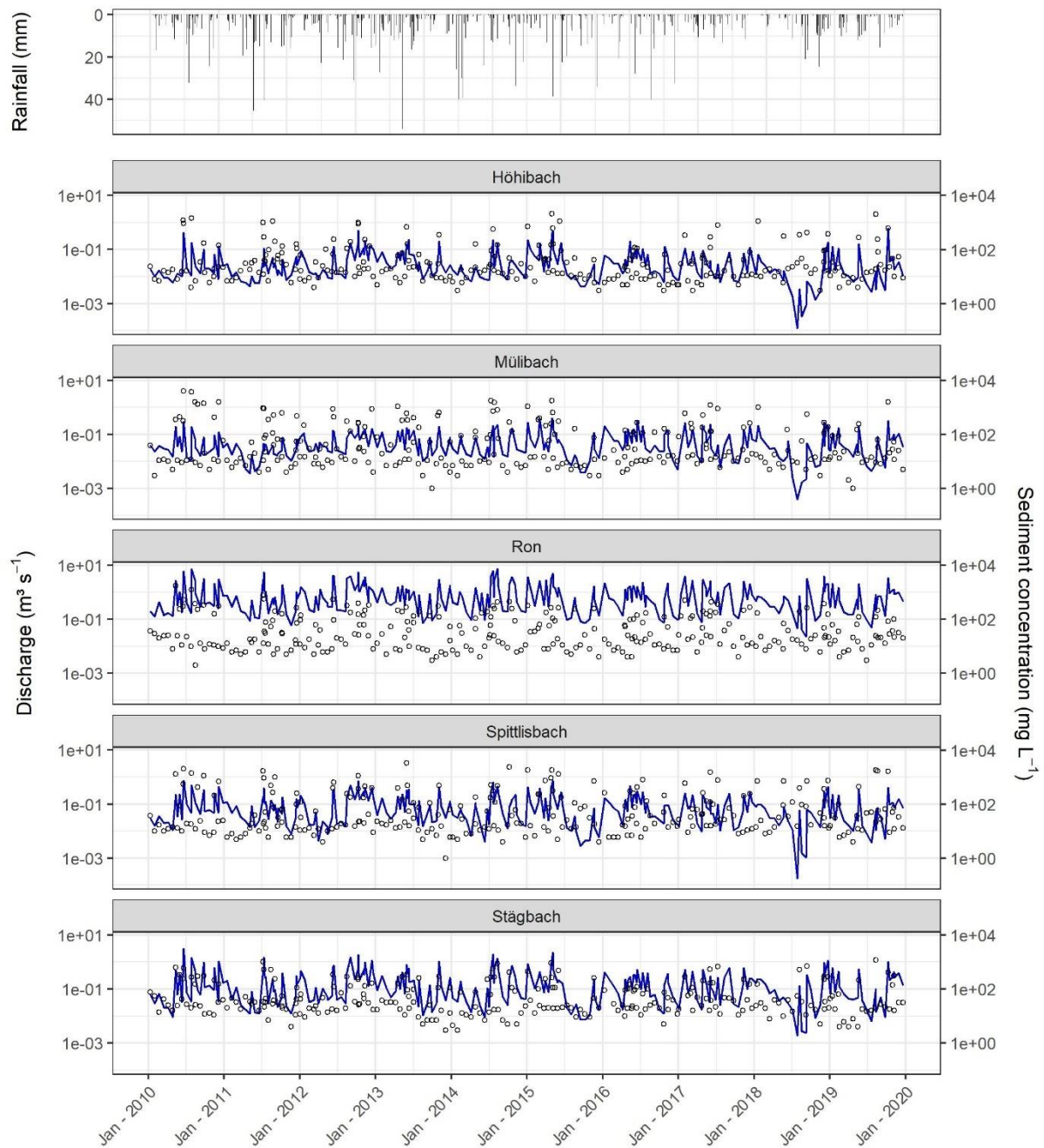
124 The elevation in the Baldegg catchment ranges from 462 to 861 m a.s.l. Steeper slopes (average values  
 125 above  $10^\circ$ ) and higher altitudes are found in the eastern and western sides of the catchment (Figure 1b),  
 126 in a typical glacial landscape of the Swiss Plateau – in this case formed by the retreat of the Reuss  
 127 Glacier in the south to north direction (~18,000 years BP) (Keller, 2021; Pfiffner, 2021). As a result,  
 128 calcareous Cambisols (IUSS Working Group WRB, 2006) developed upon Tertiary and Quaternary

129 deposits are the main soil class in the catchment. Rainfall is well distributed throughout the year,  
130 although greater precipitation is observed from May to August. The average annual rainfall (2010-2019)  
131 at the closest gauging station is  $\sim 1000 \text{ mm yr}^{-1}$  (Mosen, 454 m a.s.l.,  $\sim 3.5$  km north of the Lake Baldegg,  
132 acquired from MeteoSwiss 2021) and mean rainfall erosivity in the catchment is  $\sim 1150 \text{ MJ mm ha}^{-1} \text{ h}^{-1}$   
133  $\text{yr}^{-1}$  (Schmidt et al., 2016).

## 134 **2.2 Tributary suspended sediment loads**

135 Suspended sediment concentrations from five tributaries to the Lake Baldegg are monitored by the  
136 Department of Environment and Energy of the Canton of Lucerne. Here, we used the data measured  
137 from Jan 2010 to Dec 2019. On average 274 grab samples were taken from each tributary, which  
138 corresponds to one sample every 22 days, in addition to the samples collected during high-flow events  
139 (10 – 13 per year) (Figure 3). Suspended sediments were measured at the same location where water  
140 discharge was monitored by automatic gauging stations (Figure 1b). A summary of the measured  
141 rainfall, water discharge, and sediment concentration from 2010 to 2019 is displayed in Figure 3.





142

143 Figure 3. Daily rainfall at the Mosen station, mean daily discharge (blue line), and sediment  
 144 concentration (circles) at the monitored tributaries of the Lake Baldegg (2010-2019). Data source:  
 145 MeteoSwiss (2021).



146 In order to estimate continuous daily sediment concentration values, later used to produce average yearly  
 147 sediment loads for each tributary, we used a rating curve approach (Equation 1), combining the roughly  
 148 triweekly sediment concentration measurements with continuous discharge measurements. The rating  
 149 curve partially accounts for hysteresis and seasonality (Table 1), which can have a significant impact on  
 150 sediment export patterns and reflect the catchment landuse, hydrological connectivity, and internal  
 151 sediment source dynamics (Sherriff et al., 2016). To derive the coefficients in Equation 1 we used a  
 152 parsimonious multivariate regression which does not require separate calibration for different seasons  
 153 (Cohn et al., 1992; Vigiak and Bende-Michl, 2013).

154

$$\ln c_i = \beta_0 + \sum_{k=1}^4 \beta_k x_{k,i} + \varepsilon_i \quad (1)$$

155

156 Where:  $c$  is sediment concentration ( $\text{mg L}^{-1}$ ) for day  $i$ ,  $\beta_0$  is the intercept,  $\beta_k$  are fitted coefficients,  $x_{k,i}$   
 157 are covariates (Tab. 1) accounting for discharge, hysteresis, and seasonality,  $k$  is the covariate  
 158 identification, and  $\varepsilon_i$  is the residual error.

159 Table 1. Covariates used for fitting the sediment-rating curves, as in Vigiak and Bende-Michl (2013).

Covariate	Expression	Explanation	Physical interpretation
$x_{1,k}$	$\ln Q_i$	$Q_i = \text{discharge for day } i \text{ (m}^3\text{s}^{-1}\text{)}$	Discharge
$x_{2,k}$	$(\ln Q_i)^2$	Quadratic term of $x_{1,i}$	Hysteresis
$x_{3,k}$	$\sin(2\pi M_i/12)$	$M_i = \text{month of day } i$	Seasonality
$x_{4,k}$	$\cos(2\pi M_i/12)$	$M_i = \text{month of day } i$	Seasonality

160

161 To analyse the uncertainty in the regressions we simulated posterior distributions of the model  
 162 coefficients ( $\beta_0, \beta_k$ ) with an informal Bayesian function of the R package ‘arm’ (Gelman and Hill, 2007),  
 163 as in Batista et al. (2021). This function produces realisations of model coefficients based on the residual  
 164 standard error of the regression, which means that models with poorer fits will yield broader posterior  
 165 distributions of regression coefficients. The posterior distributions were used to simulate 1000 sediment  
 166 concentration values for each day  $i$ . These were transformed into daily distributions of sediment loads  
 167 (Mg), considering the mean daily discharge measurements from the gauging stations. Sediment loads  
 168 were ultimately aggregated into average annual values ( $\text{Mg yr}^{-1}$ ) with uncertainty bands, which should  
 169 allow for a general comparison with the different sediment connectivity scenarios simulated by  
 170 WaTEM/SEDEM.

### 171 2.3 Model description

172 A modified version of the spatially distributed erosion and sediment transport WaTEM/SEDEM (Van  
 173 Oost et al., 2000; Van Rompaey et al., 2001; Verstraeten et al., 2010) was used in this study.  
 174 WaTEM/SEDEM provides a framework for modelling sediment connectivity from hillslope to water  
 175 courses by use of a steady state transport capacity equation and a pixel-based sediment routing  
 176 component. That is, the model assumes that soil particles displaced by water erosion at a given grid cell  
 177 are transferred downstream for as long as the runoff transport capacity is greater than the sediment  
 178 supply, or until the flow path reaches a definite sink. Although the model is able to simulate both tillage  
 179 and water erosion, here we focus on the latter, which is calculated with an adaptation of the RUSLE  
 180 (Renard et al., 1997) (Equation 2). We chose to focus on soil erosion by water because in  
 181 WaTEM/SEDEM the sediment supply/routing is not affected by tillage erosion. However, tillage  
 182 erosion is likely to be an important within-field soil redistribution process in the catchment (please see  
 183 the discussion below). The model is by default executed in an average yearly time step, as typical in  
 184 RUSLE applications, which predict long-term (~20 years) average annual soil losses:

$$A = R K LS_{2d} C P \quad (2)$$

186  
 187 Where:  $A$  is average annual soil loss ( $\text{kg m}^{-2} \text{yr}^{-1}$ ),  $R$  is rainfall erosivity ( $\text{MJ mm m}^{-2} \text{h}^{-1} \text{yr}^{-1}$ ),  $K$  is soil  
 188 erodibility ( $\text{kg h MJ}^{-1} \text{mm}^{-1}$ ),  $LS_{2d}$  is a topographic factor calculated by the Desmet and Govers (1996)  
 189 procedure (dimensionless),  $C$  is a cover-management factor (dimensionless), and  $P$  is a support practice  
 190 factor (dimensionless).

191 Transport capacity ( $\text{kg m}^{-1} \text{yr}^{-1}$ ) per unit widths of grid cells is assumed to be proportional to the potential  
 192 to rill erosion, which is described by a power function of slope length and gradient (Van Rompaey et  
 193 al., 2001):

$$TC = K_{TC} RK(LS_{2d} - 4.12 S_g^{0.8}) \quad (3)$$

195  
 196 Where:  $K_{TC}$  is a landuse-dependent transport capacity coefficient (m) which requires calibration,  $R$  is  
 197 rainfall erosivity ( $\text{MJ mm h}^{-1} \text{yr}^{-1}$ ),  $K$  is soil erodibility ( $\text{t h MJ}^{-1} \text{mm}^{-1}$ ),  $LS_{2d}$  is a topographic factor  
 198 calculated by the Desmet and Govers (1996) procedure (dimensionless), and  $S_g$  is slope gradient ( $\text{m m}^{-1}$ ).  
 199

200 WaTEM/SEDEM partially incorporates the influence of the landscape structure on sediment transfer by  
 201 the use of a parcel connectivity parameter  $P_{Con}$ , which represents the proportion of sediment that is  
 202 stopped at field borders. The model also simulates runoff connectivity by means of a parcel trapping  
 203 efficiency  $P_{TEf}$  parameter, which corresponds to the proportion of the flow accumulation that is routed

204 downstream. Finally, the model is able to estimate the total amount of sediment transferred from  
205 hillslopes to water courses, which can be interpreted as the hillslope component of a catchment sediment  
206 budget. Since WaTEM/SEDEM does not represent gully and bank erosion, nor in-stream erosion and  
207 deposition processes, any comparison between modelled sediment yields and catchment-outlet sediment  
208 loads must be interpreted with caution. However, in catchments where rill and interrill are the main  
209 overland erosion processes, and assuming a state of long term fluvial quasi equilibrium, the outlet  
210 sediment loads should be at least comparable to the model outputs – even if not fully commensurable.  
211 For further information on the model, we refer to Notebaert et al., (2006), Van Oost et al., (2000), Van  
212 Rompaey et al., (2001), and Verstraeten et al., (2010).

#### 213 **2.4 Model implementation, input data, and sensitivity analysis**

214 WaTEM/SEDEM is implemented as a user-friendly GUI developed at KU Leuven (Notebaert et al.,  
215 2006). Although the software facilitates model application, it does not allow for more complex  
216 operations, such as sensitivity or uncertainty analysis. Moreover, some model components might not be  
217 fully comprehensible without access to the source code, and WaTEM/SEDEM is frequently used as a  
218 black box. Hence, in order to perform a sensitivity analysis of model parameters and underlying  
219 structural model assumptions, we implemented a WaTEM/SEDEM version using the free open source  
220 software R (R Core Team, 2021) and SAGA GIS (Conrad et al., 2015). The main adaptations are  
221 described in the following, and our code is available as supplementary material.

222 Our model application consists of a global all-at-a-time sensitivity analysis, as described by Pianosi et  
223 al. (2016). That is, we performed a Monte Carlo simulation to explore the variability of the whole  
224 parameter space, and all input factors were sampled simultaneously for each model realisation ( $n =$   
225 1200). The framework is similar to an uncertainty analysis, except in this case we did not focus on  
226 locating the parameter space which produced behavioural model realisations. Instead, we concentrated  
227 on apportioning sources of uncertainty to different model input factors, aiming to rank their contribution  
228 to the variability of the response surface (see Pianosi et al., 2016 for a review on sensitivity analysis).  
229 This should allow us to identify parameters and model assumptions that have a greater impact on the  
230 manner with which WaTEM/SEDEM describes sediment connectivity in the Baldegg catchment. In  
231 particular, the analysis of different assumptions about the structure of the model should provide a  
232 connectivity assessment based on the quantification of the structural uncertainty within the simulations.  
233 To the best of our knowledge, this is the first time the analysis of model structural error is incorporated  
234 to sediment connectivity research.

235 For each iteration of the Monte Carlo simulation, RUSLE input variables were sampled from uniform  
236 distributions (Table 2). Minimum and maximum  $R$  factor values were retrieved from the Swiss national  
237 map (Schmidt et al., 2016), and a single lumped value for the whole catchment was sampled for each  
238 iteration. The same approach was used for the  $K$  factor (Schmidt et al., 2018a). We used lumped  
239 catchment values for these factors due to their low spatial variability within the study area, according to

240 the national maps (coefficient of variations are 1% and 7% for the  $K$  and  $R$  factor, respectively). For the  
241  $C$  and  $P$  factors, here combined in a single  $CP$  parameter, uniform distributions were created for each  
242 landuse class in the catchment, based on commonly used values from the literature and a land cover map  
243 (1:25000) (Swiss Map Vector 25 BETA) (Swisstopo, 2018), which we rasterised to the model resolution  
244 (2 m x 2 m). Due to the difficulties involved in accurately representing long-term average agricultural  
245 landuse patterns and farming management practices per field parcel, pastures and cropland were  
246 considered a single arable land category, using only the information available from the land cover map  
247 (Table 2) (Swiss Map Vector 25 BETA) (Swisstopo, 2018). In this case, minimum and maximum values  
248 were relaxed to represent a wide possible combination of crops and support practices. Such  
249 combinations were assessed with the  $CP$ -Tool (Kupferschmied, 2019), which allows for the calculation  
250 of  $CP$  values considering common crop rotation systems in Switzerland. The minimum  $CP$  values were  
251 particularly reduced to include typical values for permanent grasslands in Switzerland (~0.01) (Schmidt  
252 et al., 2018b). This simplified approach should be appropriate considering i) our focus on connectivity  
253 scenarios and linear landscape structures, and ii) the use of the Monte Carlo simulation with the sampling  
254 of a wide parameter space that accounts for the uncertainty in the landuse classification. Finally, the  $LS_{2d}$   
255 factor was calculated with a slope (rad) and an upslope contributing area ( $m^2$ ) grid, which were obtained  
256 by processing a 2 m x 2 m resolution DEM from SwissALTI3D (Swisstopo, 2014a). In this case, the  
257 error in the  $LS_{2d}$  factor was not incorporated into Monte Carlo simulation due to the use of the high-  
258 resolution DEM, which should considerably reduce the uncertainty associated to the parameter  
259 estimation.

260 Table 2. Minimum and maximum parameter values sampled during the Monte Carlo simulation.

Parameter	Category	Min	Max
$R$ (MJ mm m <sup>-2</sup> h <sup>-1</sup> yr <sup>-1</sup> )		950 10 <sup>-4</sup>	1350 10 <sup>-4</sup>
$K$ (kg h MJ <sup>-1</sup> mm <sup>-1</sup> )		0.025 10 <sup>3</sup>	0.040 10 <sup>3</sup>
$CP$ (-)	Arable land	0.01	0.5
	Grass buffer strips	0.001	0.009
	Forest	0.0001	0.003
	Orchard	0.001	0.2
	Vineyard	0.05	0.6
$K_{TC}$ (m)	High (arable land, vineyard)	1	200
	Low (grass buffer strips, forest, orchard)	1	100
$P_{TEf}$ (-)		0	1
$P_{Con}$ (-)		0	1

261

262 Similarly, all WaTEM/SEDEM-specific model parameters were sampled from uniform distributions  
 263 (Table 2). Landuse classes with a  $CP$  factor above 0.01 received higher transport capacity coefficients  
 264 ( $K_{TC}$  high). The remaining landuse classes, namely forests and grass strips, received lower coefficients  
 265 ( $K_{TC}$  low). The  $K_{TC}$  reference values were taken from Van Rompaey et al. (2001) and extended in order  
 266 to explore a larger parameter space. The sampled parcel trapping efficiency ( $P_{TEf}$ ) values were assigned  
 267 to forests and grass buffer strips in the rasterised land cover map, as we explain below. The resulting  
 268  $P_{TEf}$  grid was used as a weight for calculating the aforementioned upslope contributing area. Hence, only  
 269 a proportion of the grid-cell area from forests and grass strips contributed to the downstream flow  
 270 accumulation, as runoff amounts are assumed not to increase (or to increase slowly) with slope length  
 271 under natural vegetation (Govers, 2011). Parcel connectivity ( $P_{Con}$ ) values were assigned to the forest  
 272 and grass buffer strips cells that bordered agricultural fields, representing the extent with which water  
 273 and sediment transport is reduced at parcel borders (Notebaert et al., 2006). The transport capacity (Eq.  
 274 2) at these cells was reduced by a fraction inversely proportional to the sampled  $P_{Con}$  value.

275 For each sampled combination of parameters values, the models were applied with and without the  
 276 presence of grass buffer strips between agricultural field blocks and adjacent roads and forests. Although  
 277 grass buffer strips are generally present at field borders in the Baldegg catchment (Figure 2), these  
 278 features were not distinguishable in the land cover map. Hence, we manually inserted 2 m wide grass  
 279 buffer strips at the aforementioned borders. The extent of the buffer-strips in reality is quite variable,  
 280 and generally wider at forest and river vicinities (3 – 6 m), as required by law in Switzerland (Alder et  
 281 al., 2015). For simplicity, we used a single value that should allow us to test the sensitivity of the model  
 282 to the presence of the strips. The 2 m width was selected based on the spatial resolution of the model  
 283 input data. Hedges and tree lines within field blocks were already classified in the large-scale  
 284 topographic landscape model of Switzerland (swissTLM3D) (Swisstopo, 2020) and required no  
 285 additional processing apart from a merge with the land cover map (Swiss Map Vector 25 BETA)

286 (Swisstopo, 2018). These two land surface models were combined since they contain differently  
287 assigned and complementary land cover object classes.

288 Furthermore, three road connectivity assumptions were assessed for each model iteration. For such, we  
289 first converted the roads from polylines (as available in the swissTLM3D) to polygons, using a buffer  
290 distance based on the road widths. Next, these polygons were rasterised and incorporated into the land  
291 cover grid used for modelling. In a first scenario, roads were treated as an ultimate sink, with zero  
292 transport capacity (i.e., ‘roads as sinks’). Hence, sediments reaching roads or infrastructure were  
293 subsequently removed from the system and did not reach surface waters. This represents a scenario in  
294 which roadside ditches and the road drainage system trap most sediments and partly diverge runoff to  
295 wastewater treatment plants. A second scenario assumed that all sediments reaching the road network  
296 were directly connected to the stream network. This represents a situation in which the road drainage  
297 system acts as a hydraulic shortcut, transferring sediments from fields into surface waters (i.e., ‘roads  
298 as shortcuts’) (see Schönenberger and Stamm, 2021). As in the original model formulations (see  
299 Notebaert et al., 2006), the third scenario assigned very high transport capacity to roads and  
300 infrastructure, so that no deposition would take place (i.e. ‘roads as patch connectors’). In this case,  
301 runoff and sediment might flow along or across the road network – which is expected to happen during  
302 extreme rainfall events when the drainage system is clogged. For this scenario, deposition will never  
303 occur on road cells, however sediments can still be deposited on lower patches before reaching the  
304 stream network. Hence, sediment transfer will be entirely dependent on the flow direction calculated  
305 from the DEM. Here we employed a multiple flow direction algorithm, which was used for calculating  
306 upslope contributing area and routing sediments along the flow path. The sediment routing component  
307 was implemented with a capacity accumulation function from SAGA GIS (Conrad et al., 2015), and all  
308 geo-processing tools were applied with the ‘RSAGA’ package (Brenning et al., 2018).

309 The sensitivity of WaTEM/SEDEM to the uncertainty in model parameters, the presence of grass buffer  
310 strips, and assumptions about road connectivity (i.e., model structural uncertainty) was assessed by  
311 evaluating modelled hillslope sediment yields (i.e., the amount of sediment delivered from hillslopes to  
312 surface waters) for the entire Baldegg catchment. A qualitative analysis was performed with a visual  
313 inspection of scatter plots, comparing the univariate parameter space with the model response surface.  
314 Additionally, we used a random forest analysis (RFA) to rank the importance of input factors to the  
315 uncertainty in model outputs (Antoniadis et al., 2021). That is, a random forest was used to predict the  
316 WaTEM/SEDEM-modelled sediment yields, based on the sampled parameter values for each iteration  
317 of the Monte Carlo simulation. The importance of the input factors, including model parameters, the  
318 presence of grass strips, and the road connectivity scenarios, was ranked based on their relative  
319 contribution to the RFA predictive error, following an out-of-bag estimate (Breiman, 2001). We chose  
320 the RFA due to its ability to rank both qualitative and quantitative input factors. The analysis was  
321 performed with the ‘randomForest’ (Liaw and Wiener, 2002) R package.

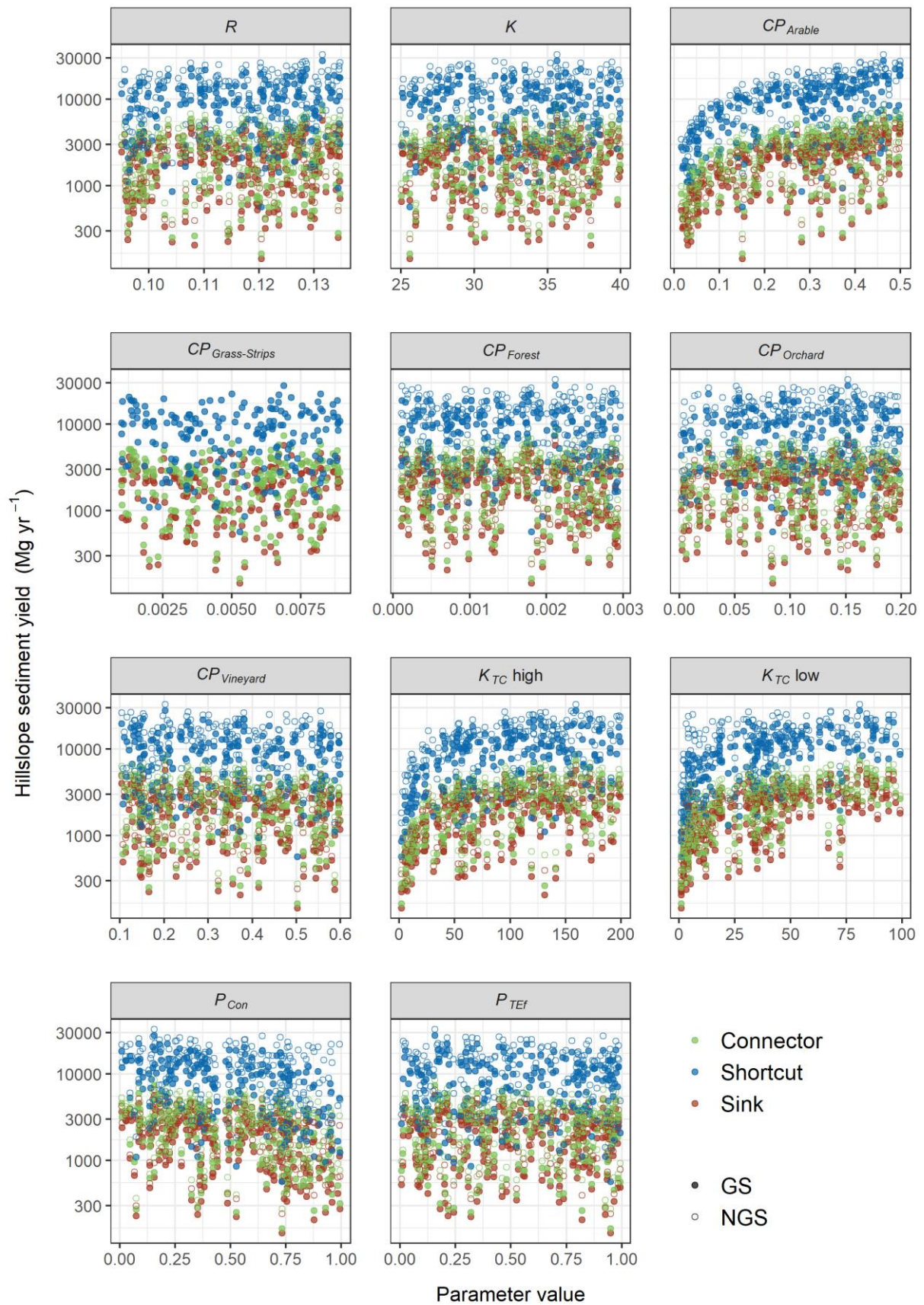


322 Finally, we compared the resulting WaTEM/SEDEM simulations of sub-catchment hillslope sediment  
323 yields to the suspended sediment loads from the monitored tributaries. Of note, with this comparison we  
324 only aim to provide a general picture of the plausibility of the model realisations. Suspended sediment  
325 loads are a product of a complex interaction of hillslope and channel remobilisation processes, which  
326 are not fully represented by WaTEM/SEDEM. In addition, since the model is RUSLE-based, the soil  
327 redistribution rates represent long-term average annual values, which hampers a straightforward  
328 comparison with annual sediment transport rates. Hence, modelled hillslope yields and suspended loads  
329 are not entirely commensurable, and we did not focus on a rejectionist framework for model testing.  
330 This research is exploratory and investigates the importance of linear features and landscape patchiness  
331 on sediment connectivity.

### 332 **3 Results**

#### 333 **3.1 Sensitivity analysis**

334 The road connectivity assumptions were by far the most sensitive input factor for WaTEM/SEDEM in  
335 the Baldegg catchment. This is illustrated in Figure 4, which presents scatter plots comparing sampled  
336 parameter values and the model response surface. The uniformly scattered points denote a low  
337 sensitivity of the modelled hillslope sediment yields to most input factors, with some evident exceptions:  
338  $CP$  for arable land,  $K_{TC}$  high, and  $K_{TC}$  low. On the other hand, all plots demonstrate that higher sediment  
339 yields were calculated when we assumed that roads behaved as hydraulic shortcuts, directly connecting  
340 agricultural patches to the stream network.

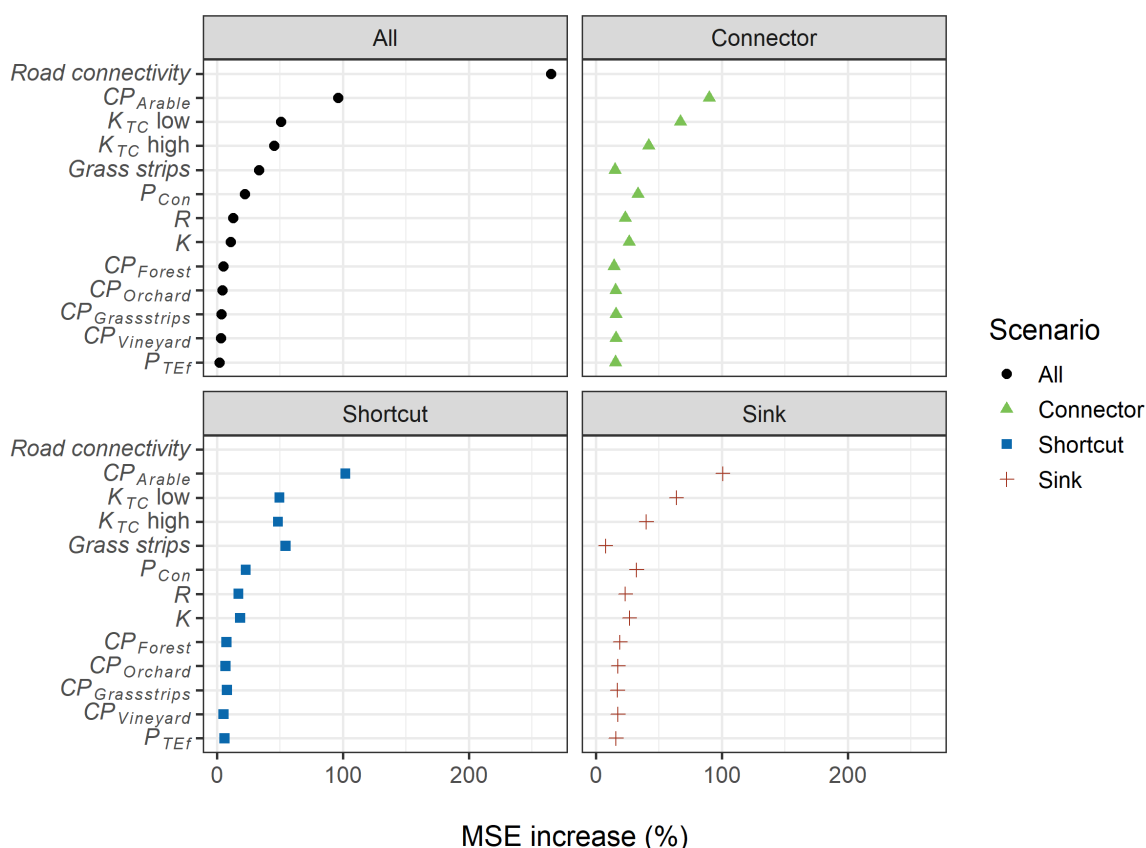


341

342 Figure 4. Univariate scatter plots of sampled parameter values. Full circles represent model realisations  
 343 with the presence of grass buffer strips (GS), and open circles represent the ones without strips (NGS).

344 Colours represent the road connectivity assumptions (i.e. 'roads as patch connectors', 'roads as hydraulic  
345 shortcuts', and 'roads as sinks'). See section 2.4 for a description of road connectivity scenarios.

346 Similarly, the results from the RFA demonstrate that road connectivity was the most important input  
 347 factor for predicting the WaTEM/SEDEM outputs (Figure 5). That is, if road connectivity was not  
 348 considered, the predictive mean squared error (MSE) of the RFA increased by 265%. The MSE increase  
 349 associated to  $CP$  for arable land (96%),  $K_{TC}$  low (51%),  $K_{TC}$  high (45%), and the presence of grass buffer  
 350 strips (33%), indicate the model was also sensitive these input factors. However, if we considered each  
 351 road connectivity scenario individually, the results from the random forest were shifted, as the model  
 352 seemed to be more sensitive to the presence of grass buffer strips for the ‘road as shortcuts’ scenario  
 353 (MSE increase = 55%).



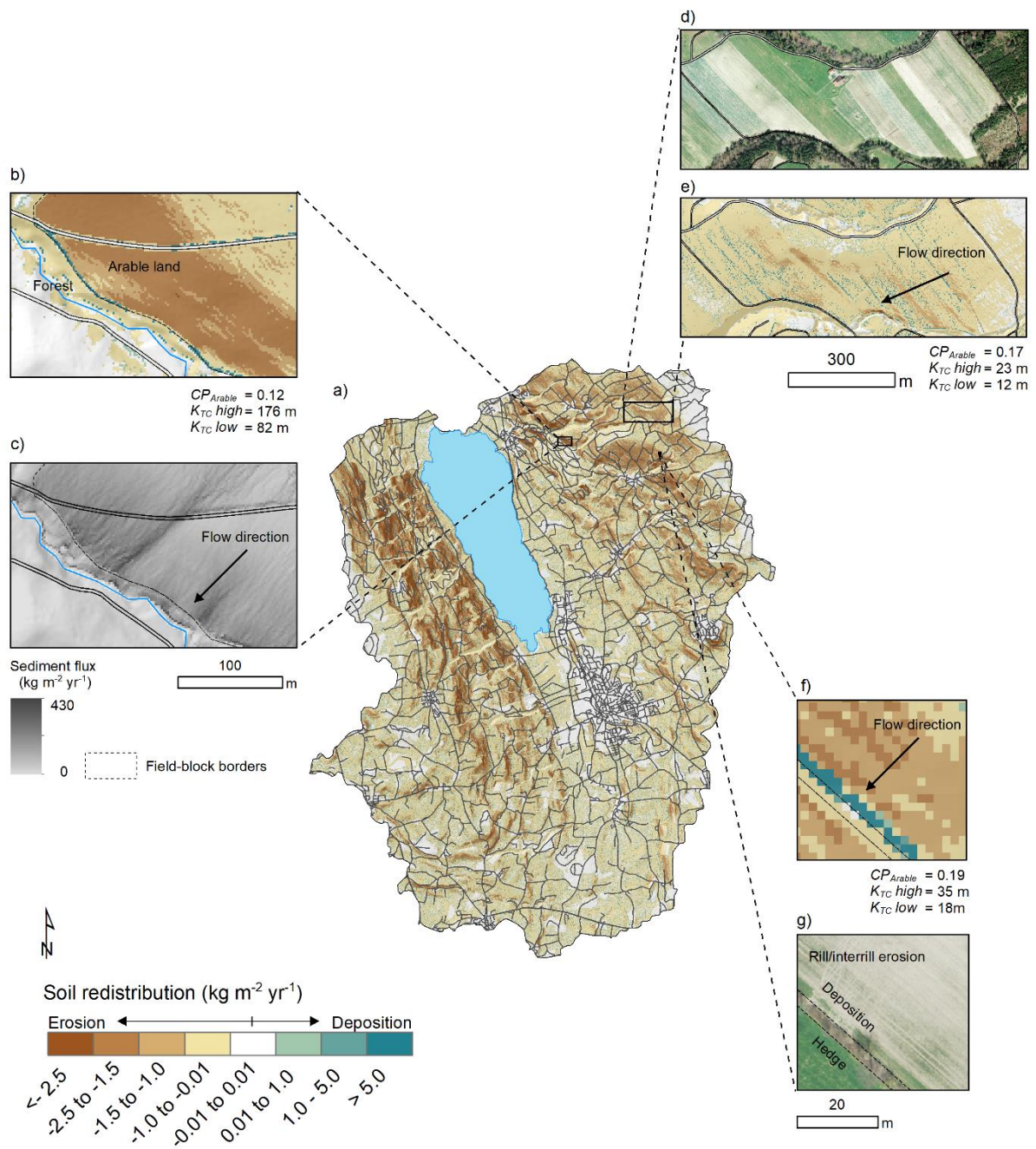
354  
 355 Figure 5. Mean squared error (MSE) increase associated to model input factors for the Random Forest  
 356 Analysis (RFA). Larger relative errors indicate the input factors were more important for estimating  
 357 model outputs.

### 358 3.2 Spatial patterns

359 The spatial patterns of soil redistribution rates were also highly influenced by linear features, landscape  
 360 patchiness, and connectivity assumptions. Sediment deposition on field blocks downslope from roads  
 361 was more frequently observed for the ‘roads as connectors’ scenario, than for the other road connectivity  
 362 assumptions. Specifically, when sediments were not diverged or trapped by the road network, there was  
 363 a greater proportion of sediment deposition on footslope field borders and other potential sinks (Figure  
 364 6b) (Table 3).







366

367 Figure 6. a) Catchment patterns of soil redistribution for a model realisation with the presence of grass  
 368 buffer strips; b) detail of sediment deposition on field borders, ‘road as patch connectors’ scenario; c)  
 369 detail of sediment fluxes across the road network, ‘road as patch connectors’ scenario’; d) detail of aerial  
 370 image of multiple parcels within a field block (Swisstopo, 2014b); e) soil redistribution rates for the  
 371 field block; f) detail of sediment deposition at a grass buffer strip at a field border; g) aerial image for  
 372 the field (Swisstopo, 2014b).

373



374 The sediment flux from agricultural fields was generally interrupted when entering forest patches, and  
 375 further deposition was modelled at forested valley floors, near the stream channels, for all scenarios  
 376 (Figure 6b, c). Importantly, sediment deposition along grass buffer strips, hedges, and tree lines reduced  
 377 sediment fluxes in between field blocks, forming a patchy connectivity pattern. This was again visible  
 378 for all simulated connectivity assumptions, albeit particularly pronounced when the presence of grass  
 379 buffer strips was considered (Figure 6 a, f).

380 Unexpectedly, the soil redistribution patterns revealed that WaTEM/SEDEM simulated linear  
 381 deposition areas at the borders of small cropland patches (Figure 6d, e). This occurred even in the  
 382 absence of grass buffer strips or hedges, and hence without  $P_{Con}$  parameterisation, which was only  
 383 applied to field-block borders. These depositional patterns were particularly evident within field blocks  
 384 oriented across the slope direction, and apparently stem from small scale changes in the slope gradient,  
 385 which were represented by the high-resolution DEM and which potentially results from long-term tillage  
 386 erosion.

### 387 3.3 Soil redistribution rates, hillslope sediment-yields, and suspended sediment loads

388 Soil redistribution rates for eroding grid cells in the Baldegg catchment were almost identical among the  
 389 simulated road connectivity assumptions (Table 3). Higher absolute deposition rates were calculated for  
 390 the simulations without grass strips for both the connector and sink scenarios, which is a result of  
 391 increased erosion rates calculated without the presence of the strips. On the other hand, lower sediment  
 392 yields were calculated with the presence of grass buffer strips when the connectivity scenarios were  
 393 analysed individually. Among these scenarios, deposition rates were lower if roads were considered to  
 394 behave as hydraulic shortcuts. Contrarily, deposition rates for the ‘roads as connectors’ and ‘roads as  
 395 sinks’ scenarios were very similar, although road deposition was only modelled in the second case.  
 396 Therefore, deposition rates within fields, patch borders, colluviums, and valley floors for the connector  
 397 scenario were ~30% higher than for the other simulations. As the sediments not diverged by the road  
 398 network were ultimately deposited within the catchment, the sink and connector scenarios displayed  
 399 very similar hillslope sediment yields. Contrarily, sediment yields for the shortcut scenario were in  
 400 general ~4.5 times higher than for the remaining road connectivity simulations.

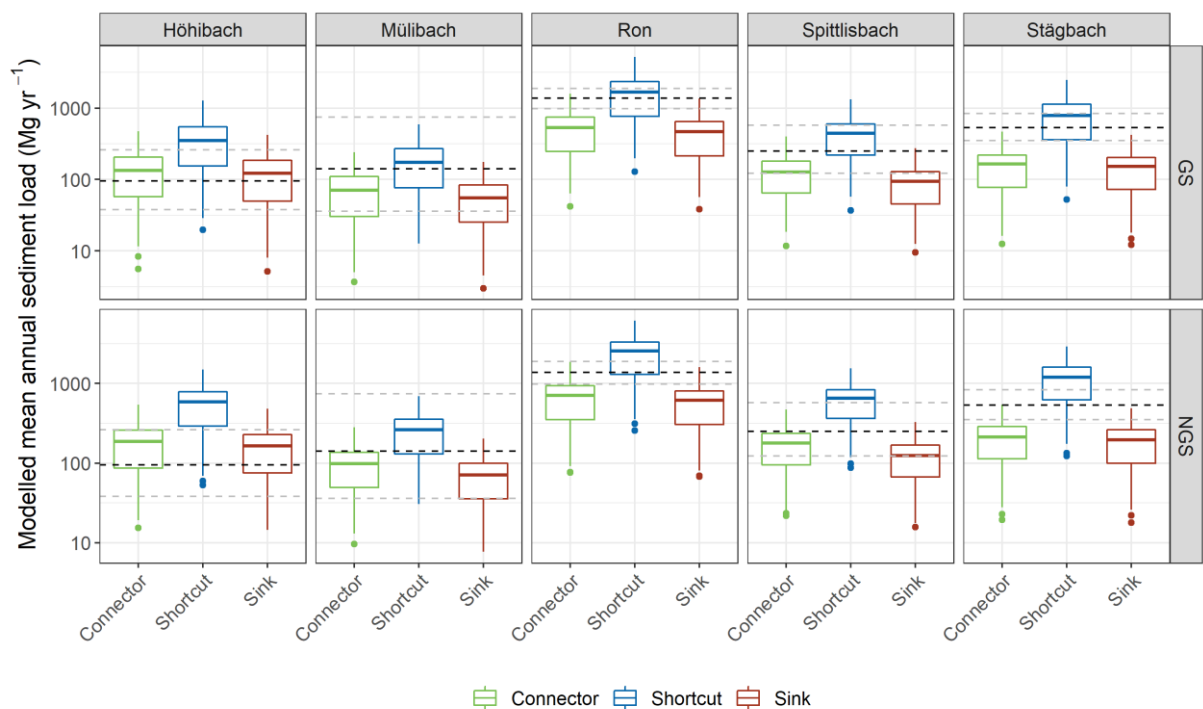
401 Table 3. Summary statistics of soil redistribution rates, hillslope sediment yields calculated by the  
 402 WaTEM/SEDEM simulations.

Scenario		Erosion			Deposition			SSY			SY		
		----- Mg ha <sup>-1</sup> yr <sup>-1</sup> -----									----- Mg yr <sup>-1</sup> -----		
		Q1	Q2	Q3	Q1	Q2	Q3	Q1	Q2	Q3	Q1	Q2	Q3
Connector	GS	3.5	6.3	8.7	3.4	5.9	8.3	0.2	0.3	0.5	1,047	2,248	3,307
	NGS	3.7	6.6	9.1	3.5	6.1	8.5	0.2	0.4	0.6	1,498	3,054	4,097
Shortcut	GS	3.5	6.3	8.8	2.7	4.9	7.2	0.6	1.2	1.8	3,878	8,467	12,242
	NGS	3.7	6.6	9.2	2.5	4.7	6.7	0.9	1.9	2.6	6,303	13,238	17,506

Sink	GS	3.5	6.3	8.8	3.4	6.0	8.4	0.1	0.3	0.4	833	1,828	2,665
	NGS	3.7	6.6	9.2	3.5	6.2	8.7	0.2	0.4	0.5	1,143	2,389	3,197

403 SSY: area specific hillslope sediment yield; SY: hillslope sediment yield. Deposition rates include  
 404 hillslope and road deposition. GS: grass buffer strips; NGS: no grass buffer strips; Q1: first quartile, or  
 405 the 25<sup>th</sup> percentile; Q2: second quartile, or the median; Q3: third quartile, or the 75<sup>th</sup> percentile.

406 The comparison between WaTEM/SEDEM simulations and the tributary sediment loads revealed a  
 407 larger overlap between the latter and the results from the ‘road as shortcuts’ scenario (Figure 7). The  
 408 overlap became particularly clear when we compared the prediction intervals of the calculations (Figure  
 409 7). That is, a smaller proportion of the ‘road as connectors’ and the ‘road as sinks’ model realisations  
 410 encompassed the tributary sediment loads, except for the Höhibach, which showed the opposite pattern.  
 411 This behaviour was particularly evident for the scenario with the presence of grass buffer strips.



412  
 413 Figure 7. Box-plots of hillslope sediment loads simulated by WaTEM/SEDEM for the road connectivity  
 414 scenarios for each tributary sub-catchment. Dashed lines represent the median (in black) and the 95%  
 415 interval (in grey) of the measurement-based estimates of sediment loads for each tributary, calculated  
 416 from the error propagation of the sediment-rating curve. GS: grass buffer strips, NGS: no grass buffer  
 417 strips. Simulations for the shortcut scenario generally shows a higher overlap with calculated sediment  
 418 loads, in particular when grass buffer strips are considered.

419 It is important to note that the median daily sediment concentrations calculated from the 1000  
 420 realisations of the rating curves (Equation 1) underestimated the high sediment concentration  
 421 measurements, for all tributaries. This resulted in the positive mean error of the median estimates (Table  
 422 4). Moreover, the Nash-Sutcliffe model efficiency coefficient for the median calculations was  
 423 unsatisfactory considering the usual thresholds for model performance (e.g. Moriasi et al., 2015).

424 However, the 95 % prediction interval of the rating curves encompassed a large proportion of the  
 425 sediment concentration observations for the tributaries with poorer fits and wider uncertainty bands (i.e.,  
 426 the Höhibach, Mülibach, and Spittlisbach) (Table 4, Supplementary Material Figure 1). The sediment  
 427 rating curves for the tributaries which displayed a better fit (i.e., the Ron and Stägbach) encompassed a  
 428 much lesser proportion of the observed sediment concentration values (Table 4, Supplementary Material  
 429 Figure 1). That is, the regressions with the lowest residual standard errors had narrower uncertainty  
 430 bands, which albeit produced more accurate median predictions, led to a greater proportion of  
 431 observations out-of-bound from the 95 % prediction interval. In any case, the largest errors were  
 432 associated to underestimates of extreme events, and therefore, it is likely that actual sediment loads from  
 433 the tributaries are contained within the long right side of the skewed distributions resulting from the  
 434 error propagation of the rating curves (Figure 7), which would increase the overlap with the shortcut  
 435 scenario.

436 Table 4. Evaluation metrics of the sediment rating curve, considering the measured sediment  
 437 concentrations and median of the simulations.

Stream	ME ----- mg L <sup>-1</sup> -----	RSME	Out-of-bound percentage* ----- % -----	r <sub>p</sub>	r <sub>s</sub>	NSE
Höhibach	56.58	80.51	13	0.51	0.61	0.20
Mülibach	96.17	142.96	14	0.56	0.72	0.24
Ron	24.18	55.42	75	0.62	0.76	0.35
Spittlisbach	108.84	155.85	29	0.46	0.63	0.14
Stägbach	33.88	68.46	51	0.47	0.68	0.15

438 \*percentage of observations out of the 95 % prediction interval. ME: mean error; RMSE: root-mean-  
 439 square error, r<sub>p</sub>: Pearson's correlation coefficient, r<sub>s</sub>: Spearman's correlation coefficient; NSE: Nash-  
 440 Sutcliffe model efficiency coefficient.

#### 441 **4 Discussion**

442 Here we assessed the interaction between landscape patchiness, linear structures, and sediment  
 443 connectivity. Our quantitative model-based approach highlighted the importance of roads in  
 444 (dis)connecting sediment fluxes between landscape compartments and surface waters in patchy  
 445 agricultural catchments. These findings are in lines with long-term field observations and qualitative  
 446 model assessments for similar areas in Switzerland.

447 For instance, Ledermann et al. (2010) monitored off-site erosion in multiple fields from different regions  
 448 of the Swiss midlands and found that linear features in general and roads in particular had a large  
 449 influence on runoff concentration, soil erosion rates, and off-site damage. These authors also estimated  
 450 that > 50 % of eroded soil was deposited in adjacent fields and infra-structure, while up to 20 % reached  
 451 surface waters, mainly through indirect inflow via the road and drainage network. Such figures are  
 452 proportionate to WaTEM/SEDEM simulations for the Baldegg catchment, specifically for the shortcut

453 scenario with the presence of grass buffer strips (Table 3). Another interesting similarity between our  
454 outputs and the field assessments from Ledermann et al. (2010), was that both approaches identified  
455 field border structures as critical regulators of soil erosion and sediment transport (see Figures 5 and 6).  
456 According to the field assessments, border furrows are specifically important for both triggering erosion  
457 and promoting diffuse sediment deposition. Such features, combined with long-term tillage erosion,  
458 might be responsible creating the topographic pattern displayed in Figure 6d.

459 Moreover, the capacity of roads to connect runoff and sediments from arable land to surface waters in  
460 Switzerland was extensively described by Alder et al. (2015) and Schönenberger and Stamm (2021).  
461 Both studies used a similar semi-qualitative modelling approach for identifying agricultural fields that  
462 were directly or indirectly (i.e. via the road and drainage networks) connected to surface waters. In  
463 particular, Schönenberger and Stamm (2021) mapped the location of drainage inlets in multiple small  
464 catchments of the Swiss Plateau. Accordingly, these authors identified the road drainage system as the  
465 main hydraulic shortcut connecting fields to water courses, as most drainage inlets discharge into surface  
466 waters (87%), and only a small proportion of them flow into wastewater treatment plants or depositional  
467 areas. Hence, the fact that the WaTEM/SEDEM ‘road as shortcuts’ scenario displayed a greater  
468 agreement with the sediment rating curves for the Baldegg tributaries (Figure 7) is coherent with the  
469 current understanding of runoff dynamics in the Swiss Plateau. Of note, the contrasting results for the  
470 Höhibach sediment loads (Figure 7), which are much closer to the sink and patch-connector simulations,  
471 do not seem to be explained by any physiographical characteristic of the sub-catchment (Supplementary  
472 Material Table 1). Hence, we speculate that this different pattern could be caused by a lower inlet  
473 drainage density or specific farming practices within the Höhibach contributing area.

474 In addition, our simulations of edge-of-field grass buffer strips indicated that these structures might be  
475 particularly relevant for the ‘road as shortcuts’ scenario. In this case, the model estimated that grass trips  
476 could reduce up to 30% the sediment connectivity from hillslopes to surface waters in the Baldegg  
477 catchment (Table 4). However, we assumed 2 m wide strips at field block borders, irrespectively of the  
478 adjacent structures or land use. As previously mentioned, the extent of these features is in fact quite  
479 variable, and legislation only requires 0.5 m filters between fields and roads, as reported by Alder et al.  
480 (2015). These authors further emphasised that albeit edge-of-field strips are an important  
481 complementary management practice, their effectiveness is often reduced in case of large drainage areas,  
482 in which very wide buffers would be necessary to stop sediment fluxes. Hence, Alder et al. (2015)  
483 recommended that minimising on-site erosion rates was ultimately the most effective way to decrease  
484 sediment input from arable land to water courses in Switzerland. Our results support this management  
485 proposition. However, our simulations also indicate that the disproportional sediment connectivity  
486 afforded by the dense road network translates into an excessive sediment supply to water courses, even  
487 when simulated erosion rates were small. As on-site erosion rates in Switzerland are already reasonably  
488 low (see Prasuhn, 2020), it might be important to consider solutions that address the sediment transport

489 through the underground drainage system, particularly in environmentally sensitive areas, such as the  
490 Baldegg catchment.

491 In a wider context, our study has demonstrated how structural sediment connectivity patterns can be  
492 investigated with a conceptual model such as WaTEM/SEDEM, provided that model spatial resolution  
493 is sufficiently fine to represent relevant features and processes. In agricultural catchments of the Swiss  
494 Plateau and likely in other patchy landscapes, soil redistribution rates and patterns are intrinsically linked  
495 to linear features (see Alder et al., 2015; Ledermann et al., 2010; Prasuhn, 2020; Remund et al., 2021).  
496 Hence, in order to provide relevant system descriptions, soil erosion models applied under similar  
497 conditions must be able to represent linear features and landscape patchiness. Although our results might  
498 seem case-specific, similar findings have been reported around the world. For instance, the effects of  
499 roads and farm tracks in both coupling and decoupling runoff and sediments has been described in  
500 Australia (Croke et al., 2005), Brazil (Bispo et al., 2020), Kenya (Stenfert Kroese et al., 2020), Italy  
501 (Persichillo et al., 2018), Spain (Calsamiglia et al., 2018), and the USA (Mahoney et al., 2018).  
502 Moreover, the influence of linear features such as field borders, hedges, terraces, and tractor tram lines  
503 on soil redistribution rates have been well documented in Europe (Calsamiglia et al., 2018b; Evrard et  
504 al., 2009; Fiener and Auerswald, 2005; Lacoste et al., 2014; Saggau et al., 2019), as well as the  
505 importance of landscape structure in regulating sediment connectivity (Baartman et al., 2020; Chartin et  
506 al., 2013; Fiener et al., 2011).

507 Another generalisable finding from our research was that WaTEM/SEDEM can be as sensitive to  
508 RUSLE parameters as to the model-specific transport capacity coefficients. Therefore, when performing  
509 uncertainty analyses of WaTEM/SEDEM, it is important to consider sources of error associated to the  
510 RUSLE parameterisation. So far, uncertainty estimation methods applied to WaTEM/SEDEM have  
511 focused on the  $K_{TC}$  parameterisation, and therefore have underestimated the uncertainty in model  
512 predictions. We anticipate that our open-source WaTEM/SEDEM script will facilitate stochastic  
513 implementations of the model, and ultimately promote uncertainty and sensitivity analysis of soil erosion  
514 models. In particular, the open-source code will allow model users to explore structural uncertainties,  
515 which can contribute to increase our understanding of sediment connectivity processes. As recent studies  
516 have again demonstrated, investigating the uncertainty in model structures, parameter estimation, and  
517 observational testing data is crucial for advancing soil erosion modelling research (Benaud et al., 2021;  
518 Eekhout et al., 2021; Schürz et al., 2020).

519 Importantly, while we demonstrated how conceptual models such as WaTEM/SEDEM can be useful for  
520 understanding structural connectivity patterns, more dynamic and process-oriented models are necessary  
521 for identifying so-called hot spots and hot moments of sediment connectivity (Owens, 2020; Turnbull  
522 and Wainwright, 2019). In addition, WaTEM/SEDEM representations of sediment transfer could be  
523 improved by incorporating the (dis)connectivity caused by linear features other than parcel borders and  
524 grass buffer strips. This might entail assimilating the  $P_{Con}$  parameter to features such as roadside ditches

525 or terraces. Finally, mapping the location of hydraulic shortcuts within the road network, as well as the  
526 extent to which these shortcuts increase the connectivity from hillslopes to water courses (e.g.,  
527 Schönenberger and Stamm, 2021), should further improve sediment connectivity simulations in areas  
528 such as the Baldegg catchment.

## 529 **5 Conclusions**

530 Here we employed a global sensitivity analysis of the WaTEM/SEDEM model to investigate the  
531 influence of linear structures and landscape patchiness on sediment connectivity in the Baldegg  
532 catchment. In particular, this novel application of WaTEM/SEDEM was implemented with the free  
533 programming language R, and our code is available as supplementary material.

534 Our results demonstrated that assumptions about road connectivity were by far the most important factor  
535 for modelling sediment transfer in the Baldegg catchment. Moreover, the comparison between extensive  
536 model simulations and sediment rating curve calculations indicated that roads and hydraulic shortcuts  
537 are likely to behave as conduits for sediment transport in the catchment. Hence, representing road  
538 connectivity is crucial for modelling sediment transfer from hillslope to water courses in this agricultural  
539 catchment of the Swiss Plateau, and potentially in other areas with a dense road drainage system.  
540 Moreover, our results further highlighted the effects of linear structures and landscape patchiness on  
541 sediment connectivity. These findings were made possible by the use of a model that was specifically  
542 tailored to explore the particularities of our study area, by effectively exploring model assumptions and  
543 the parameter space, and by the use of high-resolution spatial data.

544 Overall, we found that WaTEM/SEDEM was useful for investigating sediment connectivity in the  
545 Baldegg catchment, as it allowed us to unravel some of the processes and structures regulating hillslope  
546 sediment transport in the area. In the case the model is used for prediction and decision-making, we  
547 recommend employing a fit-for-purpose rejectionist model testing framework, with multiple sources of  
548 data, in order to evaluate the model's numerical accuracy and the quality of its spatial predictions.

## 549 **6 Code availability**

550 The code for the model simulations, sediment rating curves, and random forest analysis is available at  
551 <https://doi.org/10.5281/zenodo.6560226>.

## 552 **7 Data availability**

553 The input data for the model simulations, the raw sediment concentration and discharge data, and  
554 model results are available at <https://doi.org/10.5281/zenodo.6560226>.

## 555 **8 Author contributions**



556 PVGB and PF developed the model code, PVGB performed the simulations and analysed the data. SS  
557 prepared model input data. PVGB prepared the manuscript with contributions from all authors. CA was  
558 part of discussing ideas and revised the manuscript.

## 559 **9 Competing interests**

560 The authors declare no conflict of interest.

## 561 **10 Acknowledgements**

562 The authors would like to thank Robert Lovas, from the department of environment and energy of the  
563 Canton of Lucerne, for supplying the sediment concentration and water discharge monitoring data, and  
564 commenting on an earlier draft of this manuscript. We also appreciate the help from Axel Birkholz in  
565 acquiring the data. PVGB would like to thank Franz Conen and Claudia Mignani for their multiple and  
566 valuable inputs regarding the conceptualisation and preparation of this manuscript. We are thankful to  
567 the comments from two anonymous reviewers, which greatly improved the quality of this manuscript.

568

569 **References**

- 570 Alder, S., Prasuhn, V., Liniger, H., Herweg, K., Hurni, H., Candinas, A. and Gujer, H. U.: A high-  
571 resolution map of direct and indirect connectivity of erosion risk areas to surface waters in  
572 Switzerland-A risk assessment tool for planning and policy-making, *Land use policy*, 48, 236–249,  
573 doi:10.1016/j.landusepol.2015.06.001, 2015.
- 574 Antoniadis, A., Lambert-Lacroix, S. and Poggi, J. M.: Random forests for global sensitivity analysis:  
575 A selective review, *Reliab. Eng. Syst. Saf.*, 206, 107312, doi:10.1016/j.ress.2020.107312, 2021.
- 576 von Arb, C., Stoll, S., Frossard, E., Stamm, C. and Prasuhn, V.: The time it takes to reduce soil legacy  
577 phosphorus to a tolerable level for surface waters: What we learn from a case study in the catchment  
578 of Lake Baldegg, Switzerland, *Geoderma*, 403, doi:10.1016/j.geoderma.2021.115257, 2021.
- 579 Baartman, J. E. M., Nunes, J. P., Masselink, R., Darboux, F., Biielders, C., Degré, A., Cantreul, V.,  
580 Cerdan, O., Grangeon, T., Fiener, P., Wilken, F., Schindewolf, M. and Wainwright, J.: What do  
581 models tell us about water and sediment connectivity?, *Geomorphology*, 367, 107300,  
582 doi:10.1016/j.geomorph.2020.107300, 2020.
- 583 BAFU: Faktenblatt: Der Greifensee, Zustand bezüglich Wasserqualität, 1–8 [online] Available from:  
584 <http://www.bafu.admin.ch>, 2016.
- 585 Bakker, M. M., Govers, G., van Doorn, A., Quetier, F., Chouvardas, D. and Rounsevell, M.: The  
586 response of soil erosion and sediment export to land-use change in four areas of Europe: The  
587 importance of landscape pattern, *Geomorphology*, 98(3–4), 213–226,  
588 doi:10.1016/j.geomorph.2006.12.027, 2008.
- 589 Batista, P. V. G., Laceby, J. P., Davies, J., Carvalho, T. S., Tassinari, D., Silva, M. L. N., Curi, N. and  
590 Quinton, J. N.: A framework for testing large-scale distributed soil erosion and sediment delivery  
591 models : Dealing with uncertainty in models and the observational data, *Environ. Model. Softw.*, 137,  
592 doi:10.1016/j.envsoft.2021.104961, 2021.
- 593 Bauer, M., Dostal, T., Krasa, J., Jachymova, B., David, V., Devaty, J., Strouhal, L. and Rosendorf, P.:  
594 Risk to residents, infrastructure, and water bodies from flash floods and sediment transport, *Environ.*  
595 *Monit. Assess.*, 191(2), doi:10.1007/s10661-019-7216-7, 2019.
- 596 Benaud, P., Anderson, K., Evans, M., Farrow, L., Glendell, M., James, M. R., Quine, T. A., Quinton,  
597 J. N., Rickson, R. J. and Brazier, R. E.: Reproducibility, open science and progression in soil erosion  
598 research. A reply to “Response to ‘National-scale geodata describe widespread accelerated soil  
599 erosion’ Benaud et al. (2020) *Geoderma* 271, 114378” by Evans and Boardman (2021), *Geoderma*,  
600 402, doi:10.1016/j.geoderma.2021.115181, 2021.

601 Bircher, P., Liniger, H. and Prasuhn, V.: Aktualisierung und Optimierung der Erosionsrisikokarte (   
602 ERK2 ) Die neue ERK2 ( 2019 ) für das Ackerland der Schweiz, 2019.

603 Bispo, D. F. A., Batista, P.V.G., Guimarães, D. V., Silva, M. L. N., Curi, N. and Quinton, J. N.:   
604 Monitoring land use impacts on sediment production : a case study of the pilot catchment from the   
605 Brazilian program of payment for environmental services, *Rev. Bras. Ciência do Solo*, 44, :e0190167,   
606 2020.

607 Boardman, J.: A 38-year record of muddy flooding at Breaky Bottom: Learning from a detailed case   
608 study, *Catena*, 189(January), 104493, doi:10.1016/j.catena.2020.104493, 2020.

609 Borselli, L., Cassi, P. and Torri, D.: Prolegomena to sediment and flow connectivity in the landscape:   
610 A GIS and field numerical assessment, *Catena*, 75(3), 268–277, doi:10.1016/j.catena.2008.07.006,   
611 2008.

612 Breiman, L.: Random forests, *Machine Learning*, 45, 5-32, 2001.

613 Brenning, A., Bangs, D., Becker, M.: RSAGA: SAGA geoprocessing and terrain analysis. R package   
614 version 1.3.0., 2018.

615 Calsamiglia, A., García-Comendador, J., Fortesa, J., López-Tarazón, J. A., Crema, S., Cavalli, M.,   
616 Calvo-Cases, A. and Estrany, J.: Effects of agricultural drainage systems on sediment connectivity in a   
617 small Mediterranean lowland catchment, *Geomorphology*, 318, 162–171,   
618 doi:10.1016/j.geomorph.2018.06.011, 2018a.

619 Calsamiglia, A., Fortesa, J., García-Comendador, J., Lucas-Borja, M. E., Calvo-Cases, A. and Estrany,   
620 J.: Spatial patterns of sediment connectivity in terraced lands: Anthropogenic controls of catchment   
621 sensitivity, *L. Degrad. Dev.*, 29(4), 1198–1210, doi:10.1002/ldr.2840, 2018b.

622 Cavalli, M., Trevisani, S., Comiti, F. and Marchi, L.: Geomorphometric assessment of spatial   
623 sediment connectivity in small Alpine catchments, *Geomorphology*, 188, 31–41,   
624 doi:10.1016/j.geomorph.2012.05.007, 2013.

625 Chartin, C., Evrard, O., Salvador-Blanes, S., Hirschberger, F., Van Oost, K., Lefèvre, I., Daroussin, J.   
626 and Macaire, J. J.: Quantifying and modelling the impact of land consolidation and field borders on   
627 soil redistribution in agricultural landscapes (1954-2009), *Catena*, 110, 184–195,   
628 doi:10.1016/j.catena.2013.06.006, 2013.

629 Cohn, T. A., Caulder, D. L., Gilroy, J., Zynjuk, L. D. and Summers, R. M.: The Validity of a Simple   
630 Statistical Model for Estimating, *Water Resour. Res.*, 28(9), 2353–2363, 1992.

631 Conrad, O., Bechtel, B., Bock, M., Dietrich, H., Fischer, E., Gerlitz, L., Wehberg, J., Wichmann, V.   
632 and Böhner, J.: System for Automated Geoscientific Analyses ( SAGA ) v.2.2.2, 1991–2007,   
633 doi:10.5194/gmd-8-1991-2015, 2015.

634 Croke, J., Mockler, S., Fogarty, P. and Takken, I.: Sediment concentration changes in runoff pathways  
635 from a forest road network and the resultant spatial pattern of catchment connectivity,  
636 *Geomorphology*, 68(3–4), 257–268, doi:10.1016/j.geomorph.2004.11.020, 2005.

637 Desmet, P., Govers, G.: A GIS procedure for automatically calculating the USLE LS factor on  
638 topographically complex landscape units, *J. Soil Water Conserv.*, 51, 427–433, 1996.

639 Eekhout, J. P. C., Millares-Valenzuela, A., Martínez-Salvador, A., García-Lorenzo, R., Pérez-Cutillas,  
640 P., Conesa-García, C. and de Vente, J.: A process-based soil erosion model ensemble to assess model  
641 uncertainty in climate-change impact assessments, *L. Degrad. Dev.*, 32, 2409–2422,  
642 doi:10.1002/ldr.3920, 2021.

643 Evrard, O., Cerdan, O., van Wesemael, B., Chauvet, M., Le Bissonnais, Y., Raclot, D., Vandaele, K.,  
644 Andrieux, P. and Biielders, C.: Reliability of an expert-based runoff and erosion model: Application of  
645 STREAM to different environments, *Catena*, 78(2), 129–141, doi:10.1016/j.catena.2009.03.009, 2009.

646 Fiener, P. and Auerswald, K.: Measurement and modeling of concentrated runoff in grassed  
647 waterways, *J. Hydrol.*, 301(1–4), 198–215, doi:10.1016/j.jhydrol.2004.06.030, 2005.

648 Fiener, P., Auerswald, K. and Van Oost, K.: Spatio-temporal patterns in land use and management  
649 affecting surface runoff response of agricultural catchments-A review, *Earth-Science Rev.*, 106(1–2),  
650 92–104, doi:10.1016/j.earscirev.2011.01.004, 2011.

651 Fiener, P., Wilken, F. and Auerswald, K.: Filling the gap between plot and landscape scale – eight  
652 years of soil erosion monitoring in 14 adjacent watersheds under soil conservation at Scheyern,  
653 Southern Germany, *Adv. Geosci. Discuss.*, (July), doi:adgeo-2019-4, 2019.

654 Fryirs, K.: (Dis)Connectivity in catchment sediment cascades: A fresh look at the sediment delivery  
655 problem, *Earth Surf. Process. Landforms*, 38(1), 30–46, doi:10.1002/esp.3242, 2013.

656 Gelman, A. and Hill, J.: *Data Analysis Using Regression and Multilevel/Hierarchical Models*,  
657 Cambridge University Press, New York., R package version 1.12.2, 2007.

658 Govers, G.: Misapplications and misconceptions of erosion models, in: *Handbook of erosion*  
659 *modelling*, edited by: Morgan, R. P. C., Nearing, M.A., Blackwell Publishing Ltd., Chichester, United  
660 Kingdom, 117–134, 2011.

661 Heckmann, T., Cavalli, M., Cerdan, O., Foerster, S., Javaux, M., Lode, E., Smetanová, A., Vericat, D.  
662 and Brardinoni, F.: Indices of sediment connectivity: opportunities, challenges and limitations, *Earth-*  
663 *Science Rev.*, 187(December 2017), 77–108, doi:10.1016/j.earscirev.2018.08.004, 2018.

664 IUSS Working Group WRB. *World Reference Base for Soil Resources; IUSS Working Group WRB:*  
665 *Wageningen, The Netherlands, 2006; pp. 1–128.*

666 Keller, B.: Lake Lucerne and its spectacular landscape, in: *Landscapes and landforms of Switzerland*,  
667 edited by Reynard, E., Springer Nature Switzerland, Cham, Switzerland, 305-324, 2021.

668 Krasa, J., Dostal, T., Jachymova, B., Bauer, M. and Devaty, J.: Soil erosion as a source of sediment  
669 and phosphorus in rivers and reservoirs – Watershed analyses using WaTEM/SEDEM, *Environ. Res.*,  
670 171(January), 470–483, doi:10.1016/j.envres.2019.01.044, 2019.

671 Kupferschmied, P.: CP-Tool: Ein Programm zur Berechnung des Fruchtfolge- und  
672 Bewirtschaftungsfaktors (CP-Faktor) der Allgemeinen Bodenabtragungsgleichung (ABAG), 2019.

673 Laceby, J. P., Batista, P. V. G., Taube, N., Kruk, M. K., Chung, C., Evrard, O. and Orwin, J. F.:  
674 Tracing total and dissolved material in a western Canadian basin using quality control samples to  
675 guide the selection of fingerprinting parameters for modelling, *Catena*, 200(April 2020), 105095,  
676 doi:10.1016/j.catena.2020.105095, 2021.

677 Lacoste, M., Michot, D., Viaud, V., Evrard, O. and Walter, C.: Combining  $^{137}\text{Cs}$  measurements and a  
678 spatially distributed erosion model to assess soil redistribution in a hedgerow landscape in  
679 northwestern France (1960-2010), *Catena*, 119, 78–89, doi:10.1016/j.catena.2014.03.004, 2014.

680 Lavrieux, M., Birkholz, A., Meusburger, K., Wiesenberg, G. L. B., Gilli, A., Stamm, C. and Alewell,  
681 C.: Plants or bacteria? 130 years of mixed imprints in Lake Baldegg sediments (Switzerland), as  
682 revealed by compound-specific isotope analysis (CSIA) and biomarker analysis, *Biogeosciences*,  
683 16(10), 2131–2146, doi:10.5194/bg-16-2131-2019, 2019.

684 Ledermann, T., Herweg, K., Liniger, H. P., Schneider, F., Hurni, H. and Prasuhn, V.: Applying  
685 erosion damage mapping to assess and quantify off-site effects of soil erosion in Switzerland, *L.*  
686 *Degrad. Dev.*, 21, 353–366, 2010.

687 Liaw, A., Wiener, M.: Classification and regression by randomForest. *R News*, 2, 18–22, R package  
688 version 4.7.1, 2002.

689 Mahoney, D. T., Fox, J. F. and Al-Aamery, N.: Watershed erosion modeling using the probability of  
690 sediment connectivity in a gently rolling system, *J. Hydrol.*, 561(April), 862–883,  
691 doi:10.1016/j.jhydrol.2018.04.034, 2018.

692 Mahoney, D. T., Fox, J., Al-Aamery, N. and Clare, E.: Integrating connectivity theory within  
693 watershed modelling part I: Model formulation and investigating the timing of sediment connectivity,  
694 *Sci. Total Environ.*, 740, 140385, doi:10.1016/j.scitotenv.2020.140385, 2020a.

695 Mahoney, D. T., Fox, J., Al-Aamery, N. and Clare, E.: Integrating connectivity theory within  
696 watershed modelling part II: Application and evaluating structural and functional connectivity, *Sci.*  
697 *Total Environ.*, 740, 140386, doi:10.1016/j.scitotenv.2020.140386, 2020b.

698 MeteoSwiss. SwissMetNet Surface Weather Stations, Mosen MOA, 2010-2019 (Switzerland), 2021.

699 Müller, B., Gächter, R. and Wüest, A.: Accelerated water quality improvement during  
700 oligotrophication in peri-alpine lakes, *Environ. Sci. Technol.*, 48(12), 6671–6677,  
701 doi:10.1021/es4040304, 2014.

702 Notebaert, B., Vaes, B., Govers, G., Van Oost, K., Van Rompaey, A., and Verstraeten, G.: WaTEM /  
703 SEDEM version 2006 Manual., 2006.

704 Nunes, J. P., Wainwright, J., Biielders, C. L., Darboux, F., Fiener, P., Finger, D. and Turnbull, L.:  
705 Better models are more effectively connected models, *Earth Surf. Process. Landforms*, 43(6), 1355–  
706 1360, doi:10.1002/esp.4323, 2018.

707 Owens, P. N.: Soil erosion and sediment dynamics in the Anthropocene: a review of human impacts  
708 during a period of rapid global environmental change, *J. Soils Sediments*, 20(12), 4115–4143,  
709 doi:10.1007/s11368-020-02815-9, 2020.

710 Parsons, A. J., Wainwright, J., Brazier, R. E. and Powell, D. M.: Is sediment delivery a fallacy? Reply,  
711 *Earth Surf. Process. Landforms*, 34(February), 155–161, doi:10.1002/esp, 2009.

712 Persichillo, M. G., Bordoni, M., Cavalli, M., Crema, S. and Meisina, C.: The role of human activities  
713 on sediment connectivity of shallow landslides, *Catena*, 160(August 2016), 261–274,  
714 doi:10.1016/j.catena.2017.09.025, 2018.

715 Pianosi, F., Beven, K., Freer, J., Hall, J. W., Rougier, J., Stephenson, D. B. and Wagener, T.:  
716 Sensitivity analysis of environmental models: A systematic review with practical workflow, *Environ.*  
717 *Model. Softw.*, 79, 214–232, doi:10.1016/j.envsoft.2016.02.008, 2016.

718 Pfiffner, O. A.: The structural landscapes of Central Switzerland, in: *Landscapes and landforms of*  
719 *Switzerland*, edited by Reynard, E., Springer Nature Switzerland, Cham, Switzerland, 159-172, 2021.

720 Prasuhn, V.: Twenty years of soil erosion on-farm measurement: annual variation, spatial distribution  
721 and the impact of conservation programmes for soil loss rates in Switzerland, *Earth Surf. Process.*  
722 *Landforms*, doi:10.1002/esp.4829, 2020.

723 Remund, D., Liebisch, F., Liniger, H. P., Heinimann, A. and Prasuhn, V.: The origin of sediment and  
724 particulate phosphorus inputs into water bodies in the Swiss Midlands – A twenty-year field study of  
725 soil erosion, *Catena*, 203(March), 105290, doi:10.1016/j.catena.2021.105290, 2021.

726 Renard, K., Foster, G. R., Weesies, G. A., McCool, D. K. and Yoder, D. C.: *Predicting Soil Erosion by*  
727 *Water: A Guide to Conservation Planning With the Revised Universal Soil Loss Equation (RUSLE)*,  
728 1997.

729 R Core Team. R: A language for statistical computing. R Foundation for Statistical Computing,  
730 Vienna, Austria. URL <https://www.R-project.org>, 2021.



731 Saggau, P., Kuhwald, M. and Duttmann, R.: Integrating soil compaction impacts of tramlines into soil  
732 erosion modelling: A field-scale approach, *Soil Syst.*, 3(3), 1–28, doi:10.3390/soilsystems3030051,  
733 2019.

734 Schmidt, S., Alewell, C., Panagos, P. and Meusburger, K.: Regionalization of monthly rainfall  
735 erosivity patterns in Switzerland, *Hydrol. Earth Syst. Sci.*, 20(10), 4359–4373, doi:10.5194/hess-20-  
736 4359-2016, 2016.

737 Schmidt, S., Ballabio, C., Alewell, C., Panagos, P. and Meusburger, K.: Filling the European blank  
738 spot—Swiss soil erodibility assessment with topsoil samples, *J. Plant Nutr. Soil Sci.*, 181(5), 737–748,  
739 doi:10.1002/jpln.201800128, 2018a.

740 Schmidt, S., Alewell, C. and Meusburger, K.: Mapping spatio-temporal dynamics of the cover and  
741 management factor (C-factor) for grasslands in Switzerland, *Remote Sens. Environ.*, 211(April), 89–  
742 104, doi:10.1016/j.rse.2018.04.008, 2018b.

743 Schönenberger, U. and Stamm, C.: Hydraulic shortcuts increase the connectivity of arable land areas  
744 to surface waters, *Hydrol. Earth Syst. Sci.*, 25(4), 1727–1746, doi:10.5194/hess-25-1727-2021, 2021.

745 Schürz, C., Mehdi, B., Kiesel, J., Schulz, K. and Herrnegger, M.: A systematic assessment of  
746 uncertainties in large-scale soil loss estimation from different representations of USLE input factors—a  
747 case study for Kenya and Uganda, *Hydrol. Earth Syst. Sci.*, 24(9), 4463–4489, doi:10.5194/hess-24-  
748 4463-2020, 2020.

749 Sherriff, S. C., Rowan, J. S., Fenton, O., Jordan, P., Melland, A. R., Mellander, P. E. and Huallacháin,  
750 D.: Storm Event Suspended Sediment-Discharge Hysteresis and Controls in Agricultural Watersheds:  
751 Implications for Watershed Scale Sediment Management, *Environ. Sci. Technol.*, 50(4), 1769–1778,  
752 doi:10.1021/acs.est.5b04573, 2016.

753 Starkloff, T. and Stolte, J.: Applied comparison of the erosion risk models EROSION 3D and LISEM  
754 for a small catchment in Norway, *Catena*, 118, 154–167, doi:10.1016/j.catena.2014.02.004, 2014.

755 Stenfert Kroese, J., Batista, P. V. G., Jacobs, S. R., Breuer, L., Quinton, J. N. and Rufino, M. C.:  
756 Agricultural land is the main source of stream sediments after conversion of an African montane  
757 forest, *Sci. Rep.*, 10(1), 1–15, doi:10.1038/s41598-020-71924-9, 2020.

758 Stoll, S., Arb, C. von, Jorg, C., Kopp, S. and Prasuhn, V.: Evaluation der stark zur Phosphor-Belastung  
759 des Baldeggersees beitragenden Flächen., 2019.

760 Swisstopo. SwissALTI3D. Das hoch aufgelöste Terrainmodell der Schweiz, 2014a.

761 Swisstopo. Swissimage. Das digitale Farbornthophotomosaik der Schweiz. 2014b.

762 Swisstopo. Swiss Map Vector 25 Beta, Das digitale Landschaftsmodell der Schweiz. 2018.

763 Swisstopo. SwissTLM3D. Das grossmassstäbliche Topografische Landschaftsmodell der Schweiz,  
764 2020.

765 Teranes, J. L. and Bernasconi, S. M.: Factors controlling  $\delta^{13}\text{C}$  values of sedimentary carbon in  
766 hypertrophic Baldeggersee, Switzerland, and implications for interpreting isotope excursions in lake  
767 sedimentary records, *Limnol. Oceanogr.*, 50(3), 914–922, doi:10.4319/lo.2005.50.3.0914, 2005.

768 Turnbull, L. and Wainwright, J.: From structure to function: Understanding shrub encroachment in  
769 drylands using hydrological and sediment connectivity, *Ecol. Indic.*, 98(November 2018), 608–618,  
770 doi:10.1016/j.ecolind.2018.11.039, 2019.

771 Van Oost, K., Govers, G. and Desmet, P. J. J.: Evaluating the effects of changes in landscape structure  
772 on soil erosion by water and tillage, *Landsc. Ecol.*, 15(6), 577–589, doi:10.1023/A:1008198215674,  
773 2000.

774 Van Rompaey, A., Verstraeten, G., Van Oost, K., Govers, G. and Poesen, J.: Modelling mean annual  
775 sediment yield using a distributed approach, *Earth Surf. Process. Landforms*, 26(11), 1221–1236,  
776 doi:10.1002/esp.275, 2001.

777 Verstraeten, G., Van Oost, K., Van Rompaey, A. J. J., Poesen, J. and Govers, G.: Evaluating an  
778 integrated approach to catchment management to reduce soil loss and sediment pollution through  
779 modelling, *Soil Use Manag.*, 18(4), 386–394, doi:10.1111/j.1475-2743.2002.tb00257.x, 2010.

780 Vigiak, O. and Bende-Michl, U.: Estimating bootstrap and Bayesian prediction intervals for  
781 constituent load rating curves, *Water Resour. Res.*, 49(12), 8565–8578, doi:10.1002/2013WR013559,  
782 2013.

783 Wainwright, J., Turnbull, L., Ibrahim, T. G., Lexartza-Artza, I., Thornton, S. F. and Brazier, R. E.:  
784 Linking environmental regimes, space and time: Interpretations of structural and functional  
785 connectivity, *Geomorphology*, 126(3–4), 387–404, doi:10.1016/j.geomorph.2010.07.027, 2011.

786 Wehrli, B., Lotter, A. F., Schaller, T. and Sturm, M.: High-resolution varve studies in Baldeggersee  
787 (Switzerland): Project overview and limnological background data, *Aquat. Sci.*, 59(4), 285–294,  
788 doi:10.1007/BF02522359, 1997.

789 Wilken, F., Fiener, P. and Van Oost, K.: Modelling a century of soil redistribution processes and  
790 carbon delivery from small watersheds using a multi-class sediment transport model, *Earth Surf. Dyn.*,  
791 5, 113–124, doi:10.5194/esurf-5-113-2017, 2017.

792